AIAA JOURNAL
Vol. 34, No. 3, March 1996

Application of Absorption Filter Planar Doppler Velocimetry to Sonic and Supersonic Jets

Michael W. Smith,* G. Burton Northam,† and J. Philip Drummond*
NASA Langley Research Center, Hampton, Virginia 23681

An absorption filter planar Doppler velocimeter has been constructed and tested on a pressure-matched sonic jet and an overexpanded supersonic jet (M_{design} = 1.9). The current system can acquire single-velocity-component single-shot planar images (15-ns exposures) at 30 Hz. A unique aspect of the system is the use of a single camera and lens, made possible by the application of an image splitter system. This development reduces the expense and experimental complexity of the technique. The most extensive of the three data sets taken comprises 1100 centerline planes of instantaneous velocity acquired in the overexpanded supersonic jet. Mean and rms velocity fields are presented for this data set; a mean centerline and a mean transverse profile are extracted and compared with profiles from a computational fluid dynamics solution generated using the LARCK computer code employing a k-ϵ turbulence model.

I. Review and Introduction

IN recent years several techniques have been developed to use laser sheets to measure one or more components of flow velocity in a plane. These techniques measure velocity by one of two mechanisms: time of flight or Doppler shift. An example of a common time-of-flight technique is particle image velocimetry, a particle tracking scheme. It can provide excellent images of two instantaneous velocity components in a plane.[1] Data reduction, however, is numerically intensive, many pixels are required to produce one velocity vector (a particle must be tracked across some distance), and the technique can be thwarted by large cross-plane velocities. Several researchers have reported results using planar Doppler velocimetry (PDV) that uses Doppler shift rather than time of flight to measure velocity. In this approach, velocity is measured over an imaged plane by determining the spectral shift of light scattered from the plane. The PDV approach has several inherent advantages over the particle tracking approach. First, because a Doppler shift is measured for each pixel that is imaged, a velocity can be calculated for each pixel. This greatly increases the potential spatial resolution of the technique. Second, because no particle tracking is involved, PDV can be as sensitive to cross-plane motions as it is to in-plane motions. Finally, no special allowances need to be made to measure velocity fields that include regions of reversed flow. Positive and negative Doppler shifts are just as easily detected.

PDV results have been reported using laser-induced fluorescence (LIF), Rayleigh scattering, and Mie scattering as the signal generation processes, with both continuous wave (CW) and pulsed lasers used as the light sources.

LIF-PDV has two great advantages. First, LIF is a resonant process (i.e., the scattered light is at a specific frequency for a given molecule), allowing the velocity to be found by pumping at multiple frequencies and looking for the Doppler-shifted peak in the LIF spectrum. Second, since the flow seed is molecular, flow following is not a concern. One disadvantage is that the Doppler shift in the LIF spectrum is not just a function of flow velocity but is also a function of static pressure and temperature (this impact shift is the result of intermolecular forces). Another disadvantage is that the flow is usually seeded with noxious substances like iodine or NO that require special facilities and handling. McDaniel et al.[2] used iodine fluorescence to map the velocity field in a supersonic combustor model. They scanned their CW laser over two neighboring transitions and then fit the LIF spectrum generated for each point in the image for temperature and pressure. Knowing temperature, pressure, and the shift in the peak of each LIF spectrum, they generated corrected Doppler velocities at each point in the image. Paul et al.[3] used a different approach to deal with the unwanted dependence of the LIF Doppler shift on temperature and pressure. Working in an NO-seeded supersonic jet, they used counterpropagating laser sheets to generate separate images with positive and negative Doppler shifts. By ratioing sums and differences of these separate images, they were able to remove the thermodynamic dependence of the shift in the LIF spectrum, leaving just the Doppler dependence. Unlike the CW strategy of McDaniel et al., this approach can potentially yield single-shot velocity images.

When Rayleigh or Mie scattering is used as the signal generation process, a frequency-shift-discriminating filter must be positioned between the camera and the light sheet. The filter produces an intensity variation on the image that is related to the Doppler shift due to flow velocity. A filter is required for Rayleigh or Mie systems because they are nonresonant scattering processes. An inherent advantage of the Mie approach is that the linewidth and line shape of the scattered laser light is constant; with molecular Rayleigh, linewidth and line shape are a function of the local static pressure and temperature in the flowfield.

A cell filled with iodine vapor has been used for the frequency filter by several researchers. An iodine absorption line produces a transmission cutoff in frequency, the shape of which can be tailored by varying the pressure and temperature of the cell. Iodine has absorption lines in the tuning range of both doubled Nd:YAG lasers (532 nm) and argon-ion lasers (514 nm). Variants of such absorption filter PDV systems (henceforth referred to as AF-PDV systems) have been demonstrated.[4–9]

Komine et al.[4] presented results taken in an uncalibrated high-speed subsonic jet seeded with oil droplets (a Mie scattering experiment). Using both a CW argon-ion laser-based system and a pulsed Nd:YAG laser-based system, they demonstrated three-component velocity sensitivity. Two cameras were employed for each velocity component. One viewed the flow through an optically thin iodine filter to obtain velocity sensitivity. Their optically thin filter (defined as a filter with relatively weak line center attenuation) had a gradual cutoff, one that was nearly linear over the required range of Doppler shifts. The second camera viewed the same flow without a filter, thus providing a reference image required to normalize out the variation in seed density. Curiously, they dubbed their technique

Presented as Paper 95-0299 at the AIAA 33rd Aerospace Sciences Meeting, Reno, NV, Jan. 9–12, 1995; received Feb. 1, 1995; revision received Aug. 29, 1995; accepted for publication Oct. 30, 1995. Copyright © 1995 by the American Institute of Aeronautics and Astronautics, Inc. No copyright is asserted in the United States under Title 17, U.S. Code. The U.S. Government has a royalty-free license to exercise all rights under the copyright claimed herein for Governmental purposes. All other rights are reserved by the copyright owner.

*Aerospace Scientist, HAPB/GDD, MS 197.
†Aerospace Scientist, MS 188B. Member AIAA.

Doppler global velocimetry, even though it was an inherently planar, not volumetric, velocimeter.

Miles et al.[5] used a pulsed Nd:YAG laser, an optically thick filter, and Rayleigh scattering to examine the boundary layer in a Mach 3 wind tunnel. They called their diagnostic system filtered Rayleigh scattering (FRS). Their optically thick filter (achieved by heating the I_2 cell) had a sharp cutoff and, by definition, a strong attenuation on line center. This strong attenuation was required to suppress the scattering of non-Doppler shifted light from the tunnel walls and windows, a severe problem since Rayleigh scattering is a dramatically weaker signal generation process than Mie scattering. An advantage of the optically thick filter/Rayleigh approach is that by scanning the laser the scattered line shape can be resolved, allowing temperature as well as velocity information to be acquired, albeit only in the mean.

An FRS approach was described by Shirley and Winter[6] that eliminated the requirement of scanning the laser over the Rayleigh spectrum to determine velocity via Doppler shift. They took advantage of the dependence of the Doppler shift on viewing angle by imaging a line rather than a plane through a large aperture collection system (to get a range of viewing angles). Images of the line were spread via cylindrical optics on a two-dimensional detector producing a Rayleigh spectrum for each point in the line. These spectra could then be analyzed for velocity sensitivity.

Elliot et al.[7,8] used a Mie scattering based AF-PDV system to examine supersonic shear layers in a wind tunnel. They combined the benefits of the optically thin filter used by Komine et al. and the optically thick filters used by Miles et al. to make instantaneous planar velocity measurements without scanning the laser and without interference from light scattered by walls and windows. Employing the effects of pressure broadening on absorption line shape, they added nitrogen buffer gas to an optically thick cell to create a gradual frequency cutoff filter with deep attenuation on line center. They used this filter to replace the optically thin filter used by Komine et al. to get velocity sensitivity. The strong attenuation on line center of this hybrid filter was used to remove the scattering from walls and windows in the Doppler image. They also added a nonbroadened optically thick cell in front of the reference cell camera to remove the scattering from walls and windows from that image as well.

Meyers[9] describes the development of the Mie scattering CW argon-ion laser/30-Hz video camera approach introduced by Komine. Such systems have been successfully applied to a number of medium-to-large wind-tunnel flows at both sub- and supersonic speeds. Although useful for many wind-tunnel flows, such CW systems are not capable of producing the high temporal resolution data that pulse systems can provide for the study of turbulence and high-frequency unsteadiness. In addition CW systems have an inherent problem in flows where seeding is unsteady (i.e., time varying at a given point in the flow); large velocity bias errors may be introduced. This phenomenon is demonstrated in Sec. III.B using the averaged pulsed data from the current work to simulate CW data.

The AF-PDV system described in this paper most closely resembled the systems of Komine et al. and Elliot et al. The current system used a pulsed Nd:YAG laser operating at 30 Hz as the light source. Because jet flows were studied, scattering from walls and windows was not a concern. Thus an optically thin filter (room temperature I_2) could be employed, reducing the complexity of the experiment. A unique aspect of the present system was the use of a single camera, rather than two cameras, to measure one velocity component. This was achieved by using image splitters to place the Doppler and reference images side by side on the same camera. There are three benefits of using a single camera. The first is cost savings; especially for low-light applications where conventional $1000 charge-coupled devices (CCDs) are not acceptable, multiple camera systems can be cost prohibitive. The second is experimental simplicity (only one frame buffer required, no synching issues, no need to keep track of Doppler/reference image pairs). Third, and most important, is that the Doppler and reference images are viewed from exactly the same angle, eliminating any concern about Mie scattering lobes affecting the intensity ratio of the Doppler and reference images when taken at different scattering angles. Common viewing angle also eliminates the possibility that a dirty or scratched window might affect different portions of the Doppler and reference images; with a single camera angle, both defects would overlap and divide out during data reduction.

II. Apparatus

Figure 1 is a schematic of the optical apparatus that occupied a 4 × 8 ft tabletop. The laser was a Quanta-Ray YG-590 series 30 Hz Nd:YAG, frequency doubled to provide approximately 100 mJ per pulse at 532 nm in a 15 ns pulse, with a seeded linewidth of about 100 MHz. Note in the figure that a fraction of the green beam is split off and sent to a Burleigh RC-170 series etalon set up to operate in Fizeau mode (collimated input beam/one plate wedged). With the iodine cell in place before the etalon (dashed rectangle in Fig. 1) and the seed laser blocked (giving broadband 532 nm, about 1 cm^{-1} width), iodine absorption lines appeared as dark vertical bands on the observation screen beyond the etalon. By switching between seeded and unseeded laser operation the position of the I_2 lines relative to the narrow laser line could be quickly determined. This proved useful for orientation during calibration of the seed laser frequency tuning system (however, actual line centers were determined by slow scanning of the laser and monitoring of transmission ratio via the splitter system). The etalon was also used to monitor laser locking efficiency by visually inspecting for pedestal between the fringes during line-narrowed operation.

In Fig. 1 cylindrical lenses shape the main green beam into a two-dimensional sheet at the jet exit. The Doppler shift seen by the camera is a function of the propagation direction of the laser sheet, the viewing angle, and the magnitude and direction of the velocity according to[4]

$$\Delta v = (\hat{o} - \hat{i}) \cdot \hat{V}/\lambda \tag{1}$$

where Δv is the measured Doppler shift, $\hat{o}$ the camera viewing angle, $\hat{i}$ the laser sheet propagation direction, $\hat{V}$ the velocity, and λ the wavelength of the laser. Note that for the arrangement in Fig. 1 the system measures a velocity component that is at a 45-deg angle to the jet axis. All data presented in this paper represent this velocity component. However, all data presented were taken on the centerline of the axisymmetric jet, where the mean transverse velocity component was theoretically zero.

In front of the camera lens in Fig. 1 is the splitter system and the velocity discriminating iodine filter. Two beam splitters and two flat mirrors create two separate viewing paths, each with exactly

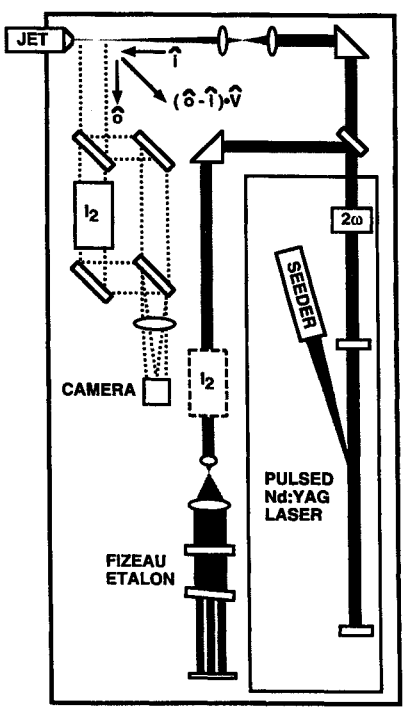

Fig. 1 Diagram of optical apparatus.

the same pathlength. The Doppler path contains an iodine filter; the reference leg does not. Between the splitter closest to the flow and the laser sheet, the two paths are carefully aligned to precisely overlap, producing exactly the same viewing angle for each path. Alignment was accomplished using an HeNe laser to trace the viewing paths through the optical splitter system.

Three different experiments, A, B, and C, were distinguished by changes/improvements in the imaging portion of the apparatus. For experiment A, only mean data and sample single-shot data could be acquired. For experiment B, data could be acquired at the laser repetition rate of 30 Hz. For experiment C, improvements were made to reduce noise and improve signal collection at the 30-Hz acquisition rate.

A liquid-cooled slow-scan low-light-level Photometrics CCD camera was employed in experiment A, an investigation of a supersonic overexpanded jet. The camera and lens (Nikon 300 mm f4.5 zoom) were mounted independently and adjusted to provide enough back focal distance to allow focusing at a magnification (image size/object size) of about one half. This camera provided very high sensitivity but was unable to acquire frames at the laser repetition rate of 30 Hz. A single frame required about 10 s to acquire, depending on the selected spatial and greyscale resolution. Mean images were generated in this experiment by leaving the camera shutter open for multiple laser shots (at f32 with ND filters); single shot images were acquired by shuttering for 1/30th of a second, exposing just one laser pulse (at f4.5, no ND filters).

For experiment B, the camera was an unintensified, shuttered CCD (Sony XC-77R) used with the same Nikon 300 mm zoom lens at f4.5. This camera operated at 30 Hz, providing an image with each laser shot. However, the lower sensitivity of this video-rate CCD could not provide images in the supersonic jet, and so data were taken in a sonic jet, where the seed density could be made much higher.

For experiment C, the same Sony XC77R was used, but this time with an f2.0 lens and a larger aperture image splitter system. The new lens was primarily employed to reduce laser speckle noise (discussed later) but also improved signal gathering capability. With this new lens and improvements in the laser sheet forming optics, signal was sufficiently increased to allow 30-Hz data acquisition in the supersonic jet.

In Fig. 2 the measured transmission curve for the room temperature (22–25°C), 20 cm pathlength iodine filter is plotted. This curve represents the lower wave number edge of the iodine line at 18787.80 cm^{-1} (532.2602 nm) convolved with the linewidth of the laser. This absorption line is not symmetric, having a more gradual slope on the lower wave number edge than on the higher wave number edge (see larger range of I_2 spectrum calculated using the code of Forkey,[10] Fig. 3). A more gradual slope is desirable for high-speed flow since it provides more dynamic range without having to pressure broaden the line with a buffer gas. The experimental spectrum in Fig. 2 was determined by tuning the laser in frequency while imaging a stationary test flow (a bit of nondairy creamer in a cell of water provided a medium with a satisfactory scattering cross section). At each frequency the average of 100 filtered and unfiltered images were ratioed (after subtracting the baseline) and then the transmission ratio was determined by taking the mean histogram value of the ratio image.

This calibration curve is valid only if the polarization of the light detected at the camera during calibration had the same polarization as the light detected at the camera during testing. This is because of the dependence of the image splitter reflectance/transmittance ratios on input polarization. If the polarizations of the laser light sheet were scrambled by the Mie scattering process (for this case, if some of the vertical were converted to horizontal), the calibration curve taken for strictly vertical polarization would be invalid. Extinction tests performed with a polarizing filter showed that both the calibration and test scattering preserved the vertical polarization of the laser, as would be expected for very small particles.

The velocity scale on the abscissa of Fig. 2 was calibrated by scanning the laser over a broad range of the iodine spectrum, between several lines of known frequency, and then converting from frequency to velocity using Eq. (1). Note that a factor of $\sqrt{2}$ has

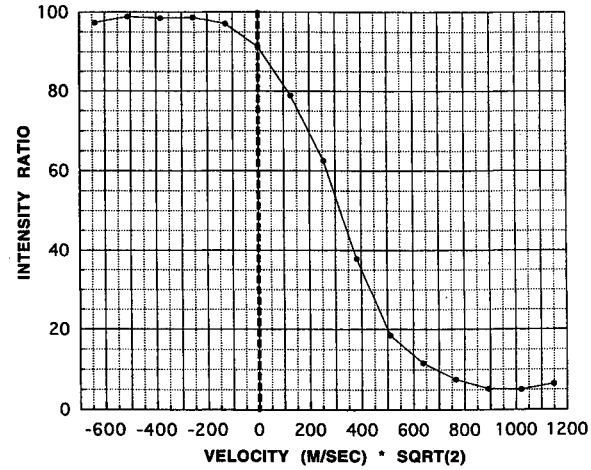

Fig. 2 Iodine cell transmission curve (20 cm and 20°C) acquired by imaging through splitter system.

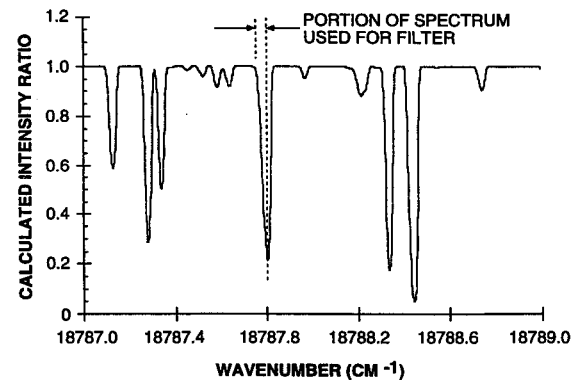

Fig. 3 Calculated absorption spectrum of iodine indicating region used for filter.

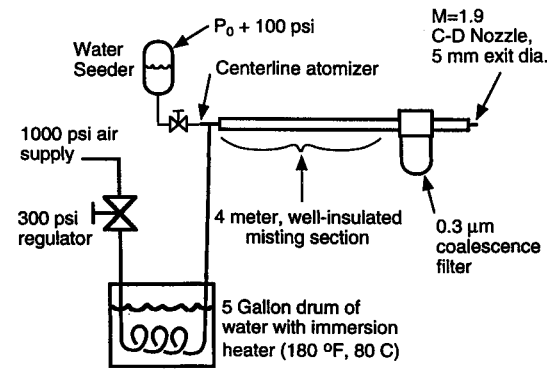

Fig. 4 Diagram of jet air supply with flow seeder plumbing.

been applied to convert from the measured component (45 deg to the jet axis) to the mean component of interest (streamwise along the jet axis). This conversion is only valid for measurements on the centerline under the assumption of axisymmetry.

In these experiments a pressure matched sonic jet and an overexpanded supersonic jet ($M_{\text{design}} = 1.9$), each with nominal exit diameters of 5 mm, were studied. Each jet was seeded the same way, by humidifying the supply air (see Fig. 4) to generate a fog of tiny droplets in the nozzle during expansion by the process of homogeneous nucleation. Note that a fine (0.3-μm) filter was included in the system to remove any droplets remaining from the humidifying process. This ensured that only the small droplets due to nucleation in the nozzle were seen in the images.

III. Data

A. Experiment A

Figure 5a shows the mean reference, mean Doppler, and resulting mean velocity image for experiment A. These images represent

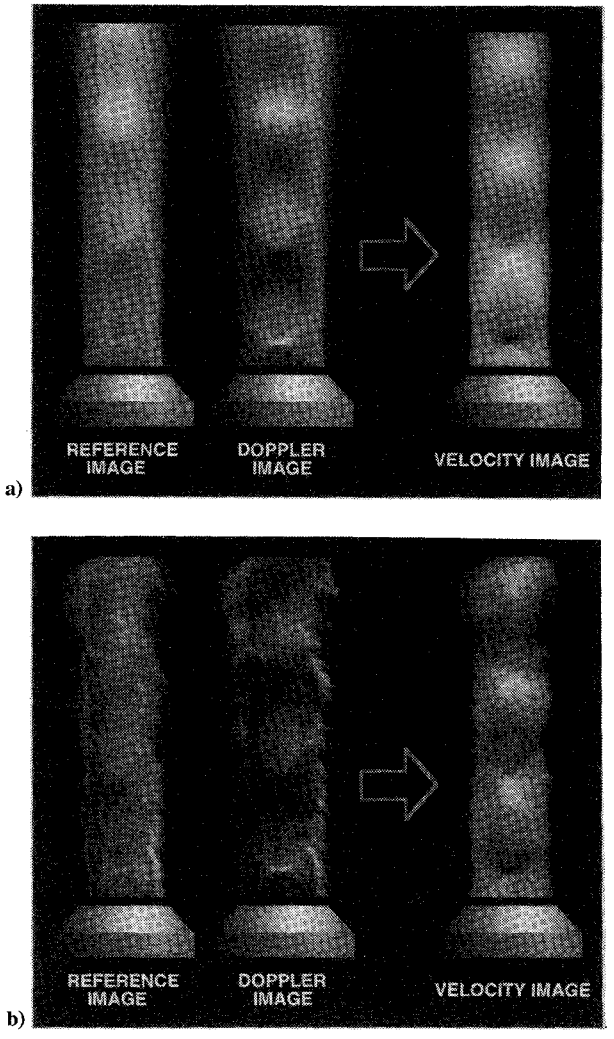

Fig. 5 AF-PDV reference, Doppler, and resultant velocity images taken with cooled, slow-scan CCD camera (experiment A): a) 900 shot average and b) single-shot (15-ns) realization.

900 laser shot averages made by opening the Photometrics camera shutter for 30 s and averaging directly on the CCD chip.

Data reduction, the process of converting the reference and Doppler images (constituting a frame of data) into velocity images was generally the same for all three experiments (A, B, and C), taking the following form.

1) A background file was generated by turning the jet seeder off and leaving the laser on. This image was subtracted from the frame to account for light on the image not due to signal generation and for the base level of the detector.

2) A gain file was generated by expanding the laser beam uniformly onto a screen using a piece of frosted glass as a diffuser. The frosted glass intercepted the laser beam about one-half meter before it reached the test region. Scattered light from the glass struck a sheet of white cardboard screen that was placed in the test region at a 45-deg angle to the beam propagation direction, allowing the illuminated screen to be visible to the camera. The image of this uniform field of light contained greyscale distortions due to etalon effects in the splitter system (producing fringe patterns on the data frames) and by nonuniform pixel gain. Each data frame was divided by this gain image to remove these effects.

3) The Doppler image was extracted from one side of the frame and slightly warped using bilinear interpolation to register exactly with the reference image on the other side of the frame. It was found that registration accuracy to a tenth of a pixel or less was required to provide good velocity images. Warping coefficients were determined interactively by aligning nodes on a grid image. The grid image was made after the run by placing a grid test pattern in the location occupied by the laser sheet during the run.

4) The Doppler image was divided by the reference image and the ratio converted from intensity to velocity using the transmission curve in Fig. 2. If the reference image had less than a predetermined level in a given pixel (about 10 counts), the velocity at that pixel was set to zero. Thus velocity was set to zero where it could not be calculated because of a lack of seed.

An instantaneous reference/Doppler/velocity image set from experiment A is shown in Fig. 5b. On the Doppler image, bright regions indicate low velocity. Note the low-speed eddies that can be seen along the edges of this instantaneous Doppler jet image.

The grainy appearance of the reference and Doppler images in Fig. 5b compared with those in Fig. 5a is because of laser speckle captured by the short laser pulse. Although similar in appearance to read noise or shot noise, three different observations demonstrated that this noise was laser speckle. First, a data image produced with laser illumination was compared with a test target image produced with white light illumination. With the same number of analog-to-digital (AD) converter counts and the same gain and collection aperture, the data target showed noise, but the test target did not. When the test target was illuminated by laser light producing the same AD count level, it then showed noise with the same spatial scales as the noisy data. Second, laser speckle noise should increase with decreasing aperture (increasing f number) according to[11]

$$\delta = \text{const} \cdot \lambda f(m+1) \tag{2}$$

where δ is an average spacing between maxima in the speckle pattern (measured in the image plane), λ is the wavelength of the laser (infinitely narrow linewidth assumed), f is the f number of the lens, and m is the magnification at which the lens is used. The observed noise on a test target was experimentally shown to increase linearly with increasing f number (at the same signal level). Finally, when the laser seeder was blocked, broadening the laser linewidth (from about 100-MHz linewidth to about 30-GHz linewidth), the noise on the target decreased, demonstrating a decrease in speckle noise with a decrease in monochromaticity. None of these three observations could be explained by either read or shot noise.

The simplest strategy for reducing the laser speckle noise is to decrease the collection f number, an approach that was used for experiment C.

B. Experiment B

Data from experiment B are shown in Fig. 6. An instantaneous planar velocity image and a 100 laser shot mean planar velocity image for the round, pressure-matched sonic jet are presented. Unlike the case of experiment A, here the mean planar image is the average of 100 processed instantaneous planar velocity images.

In Fig. 6, a region without signal appears just above each jet. This region is due to the time of flight required for the water vapor in the air to begin to condense. The nonuniformity in this interface

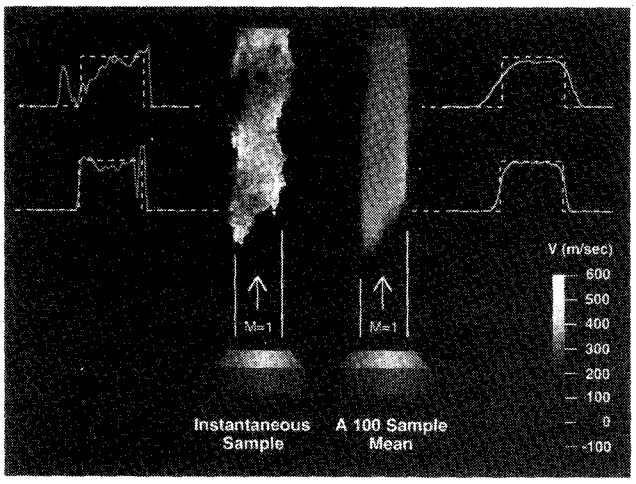

Fig. 6 Sonic jet instantaneous and mean AF-PDV data with extracted transverse profiles (experiment B).

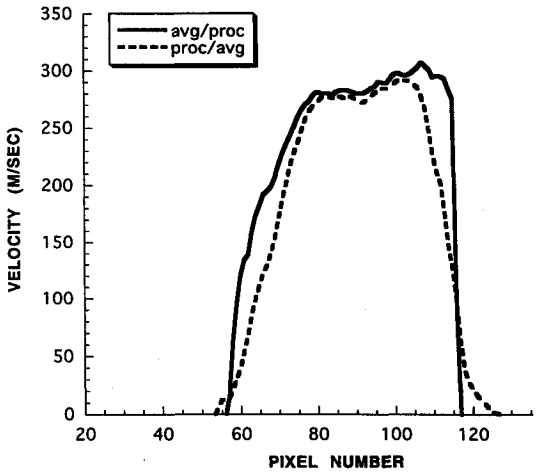

Fig. 7 Sonic jet mean velocity profiles demonstrating bias error for CW processing.

between seeded and unseeded air was due to nonuniform flow, likely caused by a bend in the supply pipe just upstream of the jet exit.

At the bottom right of Fig. 6 is a gray-scale map that can be used to translate the planar image data into velocity. To the left and right of the instantaneous and mean images, some sample profiles (solid lines) have been plotted to demonstrate agreement with the expected streamwise velocity based on isentropic flow (dashed lines).

In Fig. 7 two velocity profiles derived from the same 100 shot data set used for Fig. 6 have been plotted to illustrate the velocity bias errors that can be introduced by data averaging in turbulent flows. The dashed profile was extracted directly from the mean image in Fig. 6. It was calculated by processing each of the 100 frames, then averaging the processed instantaneous velocity images together. The solid profile was calculated by first averaging 100 frames of data to get average reference and Doppler images. Then the averaged reference and Doppler images were processed (ratioed and mapped through the filter transmission curve in the same way as the instantaneous frames) to get velocity. Thus the solid line in Fig. 7 simulates the result that would be achieved if a CW laser source were used instead of a pulsed light source. In the center of the image where the turbulent velocity fluctuations are relatively low and the seeding relatively steady, the two profiles agree well. However, in the shear layers at the edge of the jet, where the turbulent velocity fluctuations and seeding fluctuations are high, the solid profile is strongly biased to higher velocities. This is because the data reduction scheme, which uses ratioing, is nonlinear. The average of the ratio is not the same as the ratio of the average. This demonstrates that CW versions of AF-PDV can produce large errors in turbulent flows due to signal biasing caused by spatial/temporal variations in the seed concentration field.

C. Experiment C

A goal of this AF-PDV demonstration was to acquire a large database of single-shot velocity images in the supersonic overexpanded jet flow. This velocity field, which contained steady and unsteady shocks as well as large-scale turbulence and shock/turbulence interactions, could then be explored using statistical quantities such as mean, rms, and spatial cross correlation. To acquire this data the Nikon ƒ 4.5 lens used in the experiments A and B was replaced with a custom f2.0, 160-mm lens, and the aperture of the optical splitter system was correspondingly increased (80 mm maximum from 50 mm). This both reduced the speckle noise and allowed the use of a conventional 30-Hz video rate CCD. At 30 Hz, data could be acquired at the laser pulse rate for up to 180 consecutive shots [limited by the frame grabber memory (16 Mbytes)].

Experiment C produced a database of 1100 laser shots taken in 11 runs of 100 shots each. Because the total temperature (T_0) of the flow began to drop when the water droplet seeder was turned on, seeding was done in bursts of a few seconds with time allowed between 100 shot segments for T_0 to recover. Resulting nominal stagnation conditions were $T_0 = 53 \pm 2°C$, with $P_0 = 57$ psia (393 kPa) [P_0, pressure-matched operation = 90 psia (620 kPa)].

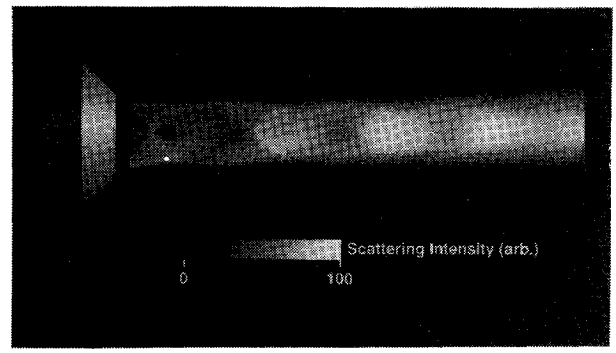

Fig. 8 Scattering intensity image for experiment C.

Figure 8 shows the 1100 shot average scattering intensity field for the jet. This image is the reference image corrected for the variations in light intensity across the laser sheet. Correction was accomplished by imaging the sheet in a calibration cell containing water and nondairy creamer. Figure 8 was generated by dividing the reference image by this calibration sheet.

Notice the dark region just downstream of the first shock on the centerline of the jet. In this region the seed droplets have begun to evaporate because of the elevated temperature behind the shock. Also note the gradual increase in scattering intensity as the jet progresses downstream. This indicates the formation of new droplets (or larger droplets) as the fluid particle time of flight increases and entrainment of cold room air increases. These features demonstrate that the scattering intensity is not an accurate indicator of the concentration of jet fluid since the droplets are clearly responding to thermodynamic changes in the flowfield. Thus the instantaneous scattering images are not very useful for quantitative mixing analysis, although they are perfectly acceptable AF-PDV reference images.

Figure 9 (top) shows the average of 1100 processed velocity images. A version of the same image reproduced with a banded gray-scale map is presented in the middle of Fig. 9. Note the extended mixing region now visible outside the core region occupied by the shock train.

At the bottom of Fig. 9 the rms image for the same 1100 shots is shown. As previously mentioned, the mean image is not sensitive to the spanwise velocity component because there is no mean spanwise motion on the jet centerline. However, the rms image includes equal sensitivity to spanwise and streamwise velocity fluctuations, per Eq. (1).

Peak rms values occur along the central portion of the mixing region seen on the mean image. Note that the shock train is visible on the rms image. This implies that the shock system is not steady; the upstream portion of the shock structure seems to vary the least, whereas the downstream portion varies the most. In the mean image this unsteadiness manifests itself as a gradual smearing of the edges of the shock diamonds as they progress downstream.

Mean profiles extracted from the mean field in Fig. 9 are presented in Figs. 10 and 11. Figure 10 shows the mean centerline profile plotted with an axisymmetric computational fluid dynamics (CFD) solution generated using the LARCK computer code employing a k-ϵ turbulence model. Also plotted for reference are the velocities determined by isentropic relations for a pressure-matched condition ($M = 1.90$ for this nozzle) and the actual overexpanded run condition used for experiment C ($M_{\text{equivalent}} = 1.54$). The data profile shows a sharp drop in velocity at the first normal shock, followed by a series of streamwise expansion and compression waves that decay with x (distance from the jet exit). Note the expected oscillation of the waves around the isentropic velocity calculated for the $M_{\text{equivalent}} = 1.54$ run condition. The preliminary LARCK code solution includes the same features. Good agreement can be seen on the location and magnitude of the normal shock, and the magnitude of the downstream wave system agrees to within 5–10%. There is some disagreement over the wavelength of the velocity oscillations. This parameter was found to be very sensitive to inflow conditions, and it is likely that the experimental exit velocity profile was not uniform as it was approximated for the CFD solution.

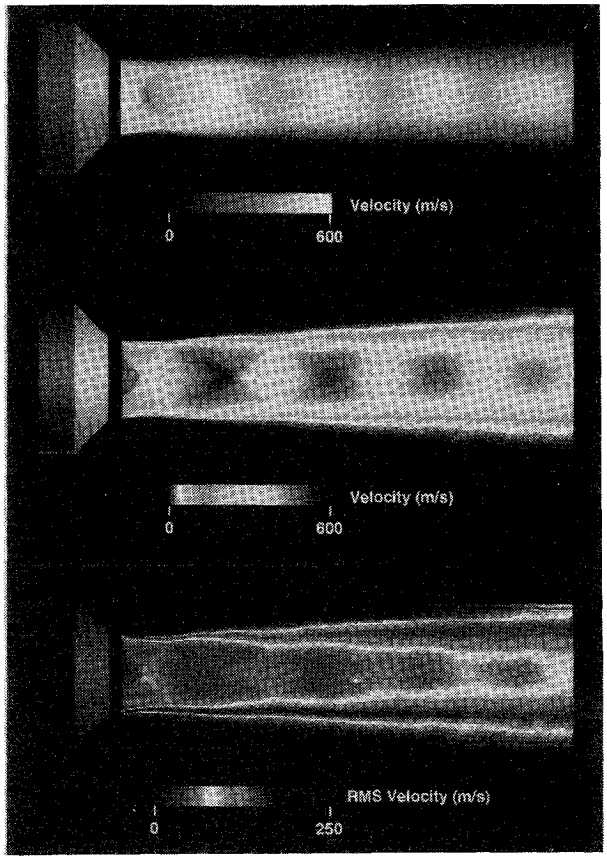

Fig. 9 Experiment C 1100 shot mean velocity field (top), same mean velocity field with banded gray-scale map (middle), and rms velocity field (bottom).

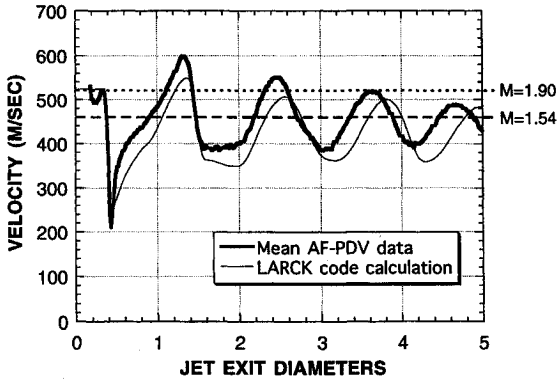

Fig. 10 Centerline mean velocity profile extracted from Fig. 9 data compared with LARCK code solution.

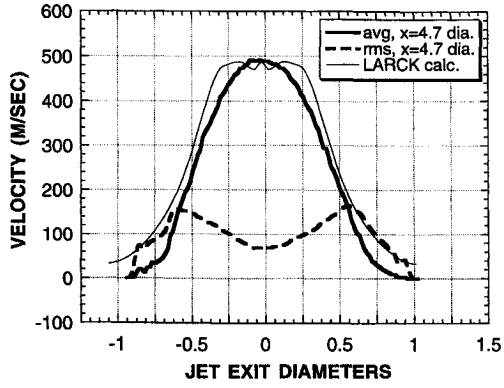

Fig. 11 Transverse mean and rms velocity profiles extracted from Fig. 9 at 4.7 diameters downstream of the jet exit, with LARCK code solution.

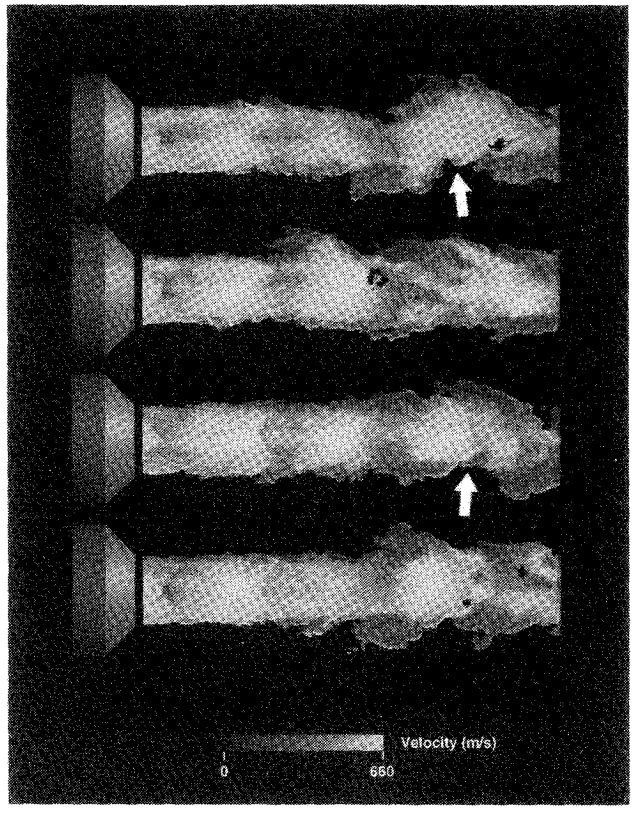

Fig. 12 Four randomly sampled single-shot instantaneous velocity fields from experiment C data set.

At pressure-matched conditions, a set of oblique waves persisted in the jet, indicating that perfectly uniform exit conditions were not possible. A more thorough analysis would include calculation of the internal nozzle flow to provide better inflow conditions to the computed domain.

Transverse mean and rms velocity profiles extracted from Fig. 9 at $x = 4.7$ nozzle diameters are shown in Fig. 11. A transverse mean profile from the LARCK solution is plotted for comparison. Taken from the $x = 5.0$ diameters position in the CFD domain (the computed velocity peak corresponding to the $x = 4.7$ diameters location on the data), this profile is in good general agreement but is somewhat fuller in both the central part of the jet as well as in the wings. The disagreement in the wings may be due to a bias in the AF-PDV data. Because only the jet fluid is seeded, some high-speed entrained room air is not represented in the average profile. Wherever data dropout occurs in a single-shot image, the velocity is set to zero, resulting in average velocities that are biased low at the edge of the jet. In the central part of the jet (−0.5 to 0.5 diameters) the disagreement may be due to either an underestimate of the turbulent mixing in the CFD solution or the aforementioned uncertainty in inflow profile. Biasing in the AF-PDV data was not a problem, since away from the jet edge, fluid was marked 100% of the time and no data dropout biasing occurred.

From the mean image in Fig. 9, it might be suggested that the jet can be thought of as a core of shock diamonds, becoming weaker in the streamwise direction, surrounded by a growing annular shear layer. This conceptual model is upset by the four sample instantaneous velocity images presented in Fig. 12. Note the bulk transverse oscillations of the jet visible at the locations indicated by arrows in the figure. These motions indicate organized large-scale unsteadiness not suggested in the mean or rms shear layer images. Also, at the second arrow in Fig. 12 (third image from the top), an isolated shock is visible. It does not appear at the characteristic angle of the shock diamond system visible further upstream and in the mean image in Fig. 9. Such shocks and their interaction with the large-scale turbulence are important features of the flow physics, yet they do not appear in the mean or rms images.

Analysis of the data set from experiment C is certainly not limited to calculation of mean and rms values. Smith and Northam[12]

performed full-field spatial correlations to investigate the unsteadiness of the shock system and the structure of the large-scale eddies. Additional calculations to investigate and quantify flow features might include higher order moments, probability distribution functions, and various forms of conditional averaging.

D. Sources of Error

The primary source of random error in the single-shot velocity images is laser speckle. A good measure of the level of this error is the rms velocity at a location in the flow where the rms should be zero. At the mouth of the jet in Fig. 9, the rms velocity is about 9% of the mean velocity. Some of this rms velocity is due to speckle noise and some is due to actual flow disturbances, although it is expected that the greater part is due to speckle. The raw Doppler and reference images exhibited speckle fluctuations of 25–30% that were reduced to a few percent before image ratioing by applying aggressive low-pass digital filtering. Of course, this approach to laser speckle reduction comes at the cost of loss of spatial resolution; other approaches do not. As noted, the simplest approach to speckle reduction is to use the lowest possible f number. For flows larger than the tiny jet studied in this test, lower magnifications and thus shorter focal lengths would be used. For such tests, f numbers approaching 1 are easily achieved (high-image-quality 50-mm focal length f1.2 lenses are inexpensive and available). Another simple means of reducing speckle in 30-Hz imaging experiments is the use of frame transfer CCD cameras as opposed to the more common interline transfer CCD, as used in the current work. Although incapable of being electronically shuttered and usually more susceptible to bloom, frame transfer CCDs have about double the active area per pixel for the same size chip (say the standard $\frac{2}{3}$ in.–8.8 mm format) reducing speckle by a factor of 2 while also increasing sensitivity. Preliminary tests show that pulse splitting can also be used as a speckle reduction scheme. Half of the laser beam is split off into a delay line (about the length of the pulse), then recombined with the main beam before the laser sheeting optics. The resulting thickened laser sheet, composed of two pulses delayed in time and slightly displaced in space, produces two speckle images that combine incoherently on the detector, cutting the measured speckle noise in half.

An important possible source of error is loss of seeder locking in the Nd:YAG laser cavity. For experiment C, the fringe pattern from a Fizeau etalon was monitored during data acquisition. If pedestal became visible between fringes, data acquisition was stopped until high locking efficiency was restored. The elimination of fringe pattern pedestal appeared to be a much better indicator of locking efficiency than stable build-up time reduction (BUT time) that was also monitored on a 1-GHz oscilloscope.

After the test series described in this paper was completed, it was discovered that poor locking efficiency control had been caused by insufficient Nd:YAG rod temperature control. The OEM cooling water regulator valve was replaced with a digital feedback controller paired with a stepping-motor-controlled valve to allow tuning of the rod temperature with the tuning of the laser frequency. This modification produced a system capable of continuous locking at any accessible frequency in the I_2 spectrum.

Another possible source of error is the drift in frequency over time of the Nd:YAG seed laser. Such a drift would produce systematic error in velocity. This was not monitored but the manufacturer's quoted specification of ± 10 MHz translates to ± 7.5 m/s, smaller than other errors.

Geometry can also produce systematic errors in measured velocity. Different regions of the flow are viewed at different angles relative to the lens and thus produce different Doppler shifts [in accordance with Eq. (1)]. For the current experiments these differences in angle are so small (less than 2 deg) that negligible changes in Doppler shift occur across the image. However, for small magnifications, i.e., flowfields much larger than the lens, a correction in the velocity calibration must be made based on viewing angle.

Many other sources of error limit the accuracy of AF-PDV measurements. For the current tests the contributions of laser dither, detector read and shot noise, and I_2 cell temperature and pressure stability to total error were assumed to be small relative to the contributions of speckle and locking efficiency. At lower velocities, on the order of tens of meters per second, these factors become important. McKenzie[13] summarizes the effects of these and other sources of error on the ultimate limits of velocity resolution with PDV systems.

IV. Conclusions

This application of AF-PDV to a sonic and an overexpanded supersonic jet illustrates the great potential of this developing technique. In the current work in which Mie scattering and an optically thin filter were employed, good velocity agreement was seen between data and calculation (both for the isentropic comparison to experiment B, Fig. 6, and the LARCK code axisymmetric turbulent solution comparison to experiment C, Figs. 10 and 11). The use of an optical splitter system allowed the use of a single camera, reducing the complexity and cost of the system as well as improving the quality of the data.

A large database (1100 centerline velocity planes, experiment A) was accumulated for a supersonic overexpanded jet. Mean and rms velocity fields were presented as well as selected instantaneous velocity fields. These showed the average shock diamond structure and shear layer growth, as well as the interaction between instantaneous shocks and the large-scale turbulent eddy motions.

Speckle noise was shown to be the largest source of random error and the reduction of speckle by decreasing f number was employed. Other laser speckle reduction schemes were discussed.

This work demonstrated the ability of this AF-PDV to acquire single-shot, single-velocity-component planar data at 30 Hz in the 100–600 m/s speed regime. With the use of absorption filters tailored by heating and pressure broadening,[7] this form of AF-PDV could be applied to lower as well as higher speed regimes. Experience from the current work suggests that at low speeds (10 m/s), accuracy will be limited by the stability of, or the ability to accurately monitor the position of, the seeded Nd:YAG laser line. At high speeds (several km/s), accuracy will be limited by the ability to find seed particles sufficiently small enough to follow the flow. In some flows, the 0.1–0.25 μm SiO_2 particles created by the combustion of silane (see Smith and Northam[14]) may prove useful. Use of such refractory particles in a jet flow would allow simultaneous quantitative concentration/velocity measurements. This is because, unlike the droplet seeding used in the current work, refractory particles would not change size in response to the thermodynamics of the flowfield.

Such particles generated by the combustion of silane would also be suitable for seeding reacting flowfields for the application of PDV. The current AF-PDV system is well suited for such an application because the interline CCD used for experiment C could be electronically shuttered to provide exposure times as short as 0.3μs. This feature would allow the rejection of the bright luminescence caused by hot seed particles in a flame, making the AF-PDV technique as suitable for high-speed combustion flows as it is for high-speed cold flows.

Acknowledgment

The authors gratefully acknowledge the work of Jeffrey A. White for his work on the CFD LARCK code solution of the supersonic overexpanded jet.

References

[1]Reuss, D. L., Adrian, R. J., Landreth, C. C., French, D. T., and Fansler, T. D., "Instantaneous Planar Measurements of Velocity and Large-Scale Vorticity and Strain Rate in an Engine Using Particle-Image Velocimetry," Society of Automotive Engineers, SAE TP 890616, Warrendale, PA, March 1989.

[2]McDaniel, J., Fletcher, D., Hartfield, R., Jr., and Hollo, S., "Staged Transverse Injection into Mach 2 Flow Behind a Rearward-Facing Step: A 3-D Compressible Test Case for Hypersonic Combustor Code Validation," AIAA Paper 91-5071, Dec. 1991.

[3]Paul, P. H., Lee, M. P., and Hanson, R. K., "Molecular Velocity Imaging of Supersonic Flows Using Pulsed Planar Laser-Induced Fluorescence of NO," *Optics Letters*, Vol. 14, No. 9, 1989, p. 417.

[4]Komine, H., Brosnan, S. J., Litton, A. B., and Stappaerts, E. A., "Real-Time, Doppler Global Velocimetry," AIAA Paper 91-0337, Jan. 1991.

[5]Miles, R. B., Forkey, J. N., and Lempert, W. R., "Filtered Rayleigh Scattering Measurements in Supersonic/Hypersonic Facilities," AIAA Paper 92-3894, July 1992.

[6]Shirley, J. A., and Winter, M., "Air-Mass Flux Measurement System Using Doppler Shifter Filtered Rayleigh Scattering," AIAA Paper 93-0513, Jan. 1993.

[7]Elliott, G. S., Samimy, M., and Arnette, S. A., "Molecular Filter-Based Diagnostics in High Speed Flows," AIAA Paper 93-0512, Jan. 1993.

[8]Elliott, G. S., Samimy, M., and Arnette, S. A., "Details of a Molecular Filter-Based Velocimetry Technique," AIAA Paper 94-0490, Jan. 1994.

[9]Meyers, J. F., "Development of Doppler Global Velocimeter for Wind Tunnel Testing," AIAA Paper 94-2582, June 1994.

[10]Forkey, J. N., private communication, Princeton Univ., Princeton, NJ, July 1992.

[11]Ennos, A. E., "Speckle Interferometry," *Laser Speckle and Related Phenomena*, 2nd ed., Springer–Verlag, Berlin, 1984, p. 207.

[12]Smith, M. W., and Northam, G. B., "Application of Absorption Filter–Planar Velocimetry to Sonic and Supersonic Jets," AIAA Paper 95-0299, Jan. 1995.

[13]McKenzie, R. L., "Measurement Capabilities of Planar Doppler Velocimetry Using Pulsed Lasers," AIAA Paper 95-0297, Jan. 1995.

[14]Smith, M. W., and Northam, G. B., "Instantaneous Planar Visualization of Reacting Supersonic Flows Using Silane Seeding," AIAA Paper 91-1690, June 1991.

SPACE ECONOMICS

Joel S. Greenberg and Henry R. Hertzfeld, Editors

This new book exposes scientists and engineers active in space projects to the many different and useful ways that economic analysis and methodology can help get the job done. Whether it be through an understanding of cost-estimating procedures or through a better insight into the use of economics in strategic planning and marketing, the space professional will find that the use of a formal and structured economic analysis early in the design of a program will make later decisions easier and more informed.

Chapters include: Financial/Investment Considerations, Financial/Investment Analysis, Cost Analysis, Benefit/Cost and Cost Effectiveness Models, Economics of the Marketplace, Relationship of Economics to Major Issues

AIAA Progress in Astronautics and Aeronautics Series

1992, 438 pp, illus, ISBN 1-56347-042-X
AIAA Members $59.95 Nonmembers $79.95
Order #: V-144(830)

Place your order today! Call 1-800/682-AIAA

AIAA

American Institute of Aeronautics and Astronautics

Publications Customer Service, 9 Jay Gould Ct., P.O. Box 753, Waldorf, MD 20604
FAX 301/843-0159 Phone 1-800/682-2422 8 a.m. - 5 p.m. Eastern

Sales Tax: CA residents, 8.25%; DC, 6%. For shipping and handling add $4.75 for 1-4 books (call for rates for higher quantities). Orders under $100.00 must be prepaid. Foreign orders must be prepaid and include a $25.00 postal surcharge. Please allow 4 weeks for delivery. Prices are subject to change without notice. Returns will be accepted within 30 days. Non-U.S. residents are responsible for payment of any taxes required by their government.